Computer-aided Diagnosis of Retinopathy of Prematurity via Analysis of the Vascular Architecture in Retinal Fundus Images of Preterm Infants

Faraz Oloumi[1], Rangaraj M. Rangayyan[1] and Anna L. Ells[1,2]
[1]*Department of Electrical and Computer Engineering, Schulich School of Engineering, University of Calgary, Calgary, AB, Canada*
[2]*Division of Ophthalmology, Department of Surgery, Alberta Children's Hospital, Calgary, AB, Canada*

1 RESEARCH PROBLEM

Retinopathy of prematurity (ROP) is a disorder that affects the development of blood vessels in the retina of premature infants, and is the leading cause of preventable childhood blindness (International Committee for the Classification of Retinopathy of Prematurity, 2005). Because advanced ROP can progress rapidly in the first 8 to 12 weeks of life, prompt identification of high-risk features of the disease is critical to the management of the affected infants. The posterior signs that are indicative of the presence of ROP are the straightening of the major temporal arcade (MTA), a decrease in the angle of insertion of the MTA, and increased dilation and tortuosity of the arteriole and venular vessels (International Committee for the Classification of Retinopathy of Prematurity, 2005; Cryotherapy for Retinopathy of Prematurity Cooperative Group, 2001; Wilson et al., 2006; Wong et al., 2011; Wilson et al., 2008).

The presence of plus disease can be indicative of the severity of active ROP. Plus disease is diagnosed by the presence of a certain amount of increase in venular dilation and arteriole tortuosity in at least two quadrants of the eye (International Committee for the Classification of Retinopathy of Prematurity, 2005). The presence of sufficient dilation and tortuosity of the posterior vessels for the diagnosis of plus disease is determined by visual comparison to a gold standard retinal fundus photograph (International Committee for the Classification of Retinopathy of Prematurity, 2005; Watzke et al., 1990; Wilson et al., 2008). A severe form of ROP, called aggressive posterior ROP, shows increase in the dilation and tortuosity of the blood vessels in all four quadrants at early stages of its development (International Committee for the Classification of Retinopathy of Prematurity, 2005).

The angle of insertion of the MTA has been loosely defined as the angle between the superior and inferior temporal arcades (STA and ITA) as they diverge from the optic nerve head (ONH) and extend towards the periphery of the retina (Wilson et al., 2006; Cryotherapy for Retinopathy of Prematurity Cooperative Group, 2001). Despite the clinical importance of abnormal changes in the architecture of the MTA, only the angle of insertion of the MTA has been quantified manually in only two studies dealing with ROP (Wilson et al., 2006; Wong et al., 2011).

Treatment of ROP is primarily driven by the identification of the above-mentioned features via clinical examination or photographic documentation. The current clinical method for diagnosis of plus disease is subjective. As shown by Chiang et al. (Chiang et al., 2007), among 22 recognized ROP experts who performed diagnosis of plus disease on 34 images of preterm infants based on a three-level classification (plus, preplus, and neither), the experts agreed on the diagnosis of only 12% of the images (four out of 34). It is likely that no optimal visual reference standard exists for the diagnosis of plus disease, as shown by disagreement even among recognized experts (Chiang et al., 2007; Wallace et al., 2008). Such studies show the need for computer-aided methods to quantify the changes in retinal blood vessels in the presence of plus disease. Computer-aided diagnosis (CAD) and quantitative analysis of the vascular architecture of the retina could assist in monitoring the evolution and stages of ROP, their effects on the visual system, and the response to treatment.

2 OUTLINE OF OBJECTIVES

The aim of the proposed thesis is the derivation of various diagnostic features and measures to perform CAD of ROP in retinal fundus images of preterm infants. Diagnostic parameters characterizing the vascular architecture, in terms of quantification of the openness of the MTA, as well as measurements of the thickness and tortuosity of the blood vessels, will be derived and analyzed to follow quantitatively the effects of pathology on retinal vessels, as well as the

Oloumi F., Rangayyan R. and Ells A..
Computer-aided Diagnosis of Retinopathy of Prematurity via Analysis of the Vascular Architecture in Retinal Fundus Images of Preterm Infants.

effects of treatment in ROP cases. The methods will be tested with an established longitudinal database {Telemedicine for ROP In Calgary (TROPIC) (Hildebrand et al., 2009)}, available at the Alberta Children's Hospital. The results will be evaluated quantitatively by comparing against delineation of the corresponding features by an expert ophthalmologist (Dr. A. L. Ells). Quantitative models correlating the obtained parameters with the effects of pathology and treatment will be derived and verified.

3 STAGE OF THE RESEARCH

The present research study has passed the preliminary stages of planning and review and is at the stage of implementation of the proposed methodology with some initial results already obtained. The current state-of-the-art methodology, or lack thereof, has been established and reviewed and based on this, new and novel methodology is proposed, as explained in Section 5.

4 STATE OF THE ART

The proposed thesis and its underlying research work consists of quantification of the openness of the MTA, as well as thickness and tortuosity of the vessels. The current state-of-art methods relating to the computation of each parameter are reviewed in the following sections.

4.1 Measurement of the Angle of Insertion of the MTA

Wilson et al. (Wilson et al., 2006) measured the angle of insertion of the MTA as follows: the center of the ONH and the fovea are manually marked by two independent observers. A line is drawn through the manually marked centers of the ONH and the fovea; this is the retinal raphe. The image is rotated so that the retinal raphe is horizontal. A line perpendicular to the retinal raphe is drawn from the fovea until it intersects the ITA and the STA. From the intersections, two lines are drawn to the center of the ONH. The total arcade angle (TAA) is defined as the sum of the inferior and the superior arcade angles (IAA and SAA). A significant level of acuteness in the IAA of the left eye was associated between stage 0 and 1, stage 1 and 2, and stage 1 and 3 of ROP (higher numbers indicate higher severity of ROP).

In a follow-up study by Wong et al. (Wong et al., 2011), semiautomated measurements were made of four angles of the temporal and the nasal venules and arterioles. The procedures required manual editing of automatically detected vessels. The vertex of all angles was set at the center of the ONH, and the other two points were obtained automatically as the intersection of a circle of radius 60 pixels with the previously marked major arteriole and venule branches on both the temporal and the nasal sides. The angles of the temporal venules and arterioles were found to have statistically significant differences between normal cases and stage 3 ROP. However, when all stages of ROP were combined, only the angle of the temporal arterioles indicated statistically significant difference as compared to the normal cases.

Ells and MacKeen (Ells and MacKeen, 2008) illustrated that the changes that occur in the MTA in the presence of ROP are dynamic as they alter the posterior architecture of the MTA. Based on this, we believe that the arcade angle measures proposed by Wilson et al. (Wilson et al., 2006) and Wong et al. (Wong et al., 2011) may not accurately reflect such changes that occur over the entire posterior architecture of the MTA, as they only define the openness of the MTA based on three points and the methods are similar to fitting a triangle to the MTA. Furthermore, only the location of the vertex of the arcade angle has been consistently defined as the center of the ONH; the locations of the other two points have been defined in different manners. Moreover, the value of the arcade angle is sensitive to the location of the center of the ONH provided by the user; a difference of 10 pixels in the location of the marked center of the ONH can result in a difference of 10° in the measured arcade angle.

4.2 Measurement of Vessel Thickness and Tortuosity

Using a binary vessel map, Heneghan et al. (Heneghan et al., 2002) computed the vessel width by extending a line segment, in different directions, from a pixel that belongs to the vessel on both sides in opposite directions until nonvessel pixels were encountered. The width of the vessel was taken as the smallest distance over all angles. Heneghan et al. also obtained the tortuosity of the vessels by first dividing a vessel into smaller linear segments and then dividing the total length of a vessel by the length of its chord.

Wilson et al. (Wilson et al., 2008) measured the vessel width using two different methods. As one measure, the standard deviation of the Gaussian profile that was used to detect the blood vessels was used. As a second measure, the correlated measure of to-

tal isotropic contrast at the vessel center-line along the entire length of the vessel was used. Wilson et al. (Wilson et al., 2008) also measured the tortuosity of a blood vessel by dividing a vessel segment into smaller segments using the bisector of each segment and the length of their chords until a minimum chord length was reached. The tortuosity of the vessel was computed by considering the change in the chord length after division of each segment into two parts.

Fiorin and Ruggeri (Fiorin and Ruggeri, 2011) proposed semiautomated methods for measurement of vessel thickness and tortuosity in narrow-field retinal fundus images of preterm infants using a web-based graphical user interface (GUI). The center-line of the vessel to be analyzed was selected manually and the edges of the vessel were extracted using the Canny filter. The vessel width and tortuosity were then computed using the center-line and by associating pairs of points on opposite edges so that a line through the two points would be perpendicular to the vessel center-line.

By finding the branching and the end points of a vessel skeleton map, Gelman et al. (Gelman et al., 2005) divided a vessel into smaller segments. The tortuosity was measured as the sum of the length of all such segments divided by the length of the chord of the entire vessel. The width of the vessel was measured as its total divided by its length.

Poletti et al. (Poletti et al., 2012) used various forms of vessel-level tortuosity such as angle-based tortuosity, caliber-weighted angle-based tortuosity, and twisted-based tortuosity to derive eight different measures of tortuosity. A linear weighted combination of the eight different measures was then obtained to represent an image-level tortuosity measure for each image.

4.3 Detection of the MTA for the Localization of other Anatomical Features

Because the MTA originates from the ONH and follows a curved, almost parabolic, path towards the macula, it can be used to detect or estimate the position of the ONH. Furthermore, relative to the location of the ONH, the macular region can also be estimated or detected (Foracchia et al., 2004; Li and Chutatape, 2004; Tobin et al., 2007; Fleming et al., 2007; Ying and Liu, 2010).

Using an estimate of the ONH location and a binarized image of the vasculature, Tobin et al. (Tobin et al., 2007) proposed to apply a parabolic model to the statistical distribution of a set of points given by a morphologically skeletonized vascular image to find an estimate of the retinal raphe. A parabola of the form $ay^2 = |x|$ was modified to accommodate for the shifted vertex at the most likely ONH location and the angle of rotation of the retinal raphe, β. The resulting model and the skeletonized image were used with a least-squares method to estimate the parameters a and β. Even though Tobin et al. estimated the openness of the parabolic model, it was only used to draw a parabola on the image.

Fleming et al. (Fleming et al., 2007) proposed a method to extract the MTA by means of vessel enhancement and semielliptical curve fitting using the generalized Hough transform (GHT). First, the vessels were enhanced to get a magnitude image and a phase image of the vascular architecture. Assuming that, having an edge map and knowing the orientation of the arcade, a reference point can only be at one of a few locations, the GHT was applied to a skeletonized image of the vasculature. The Hough space dimension was set to be five, with variables for inclination, horizontal axis length, left or right opening, and the location of the center of the ellipse. Anatomical restrictions were applied to the variables to limit the number of semiellipses generated by the method. The global maximum in the Hough space was selected as the closest fit to the MTA.

Ying and Liu (Ying and Liu, 2010) obtained a vascular topology map using an energy function defined as the normalized product of the local blood vessel width and density. A quantile threshold was used on the vascular topology map to extract the pixels in a high-energy band. A circle-fitting method was applied to the extracted pixels to model the MTA as a circle, which was then used to localize the macula.

By using the supremum of openings operator on an enhanced grayscale image of blood vessels, Welfer et al. (Welfer et al., 2010) extracted the STA and the ITA to locate the center of the optic nerve head (ONH). A set of 24 linear structuring elements of length 80 pixels was used to extract the MTA. The resulting image was binarized, skeletonized, and pruned to obtain a binary image that represented the STA and the ITA.

Even though the structure of the MTA has been used to estimate the ONH and the macula in previously reported works, only Tobin et al. modeled the arcade for parametrization of its openness; however, they used the openness parameter only to draw the parabolic model on the image.

5 METHODOLOGY

5.1 Previously Conducted Work

This section provides a description of the preliminary work that has been conducted to date and tested based on the proposed thesis objectives. These include, but are not limited to, algorithms for the detection of retinal vessels, algorithms for the detection and modeling of the MTA, and design of a GUI to facilitate the for implementation and application of the proposed methods in a clinical setting.

5.1.1 Detection of Blood Vessels

Real Gabor filters, which are optimal for the detection of piecewise linear and oriented features, are used for the detection of the blood vessels (Rangayyan et al., 2008). The preprocessing steps for vessel detection include:

1. Normalizing each color component in the original image.
2. Computing the luminance component.
3. Thresholding the luminance component to obtain the effective area.
4. Extending the luminance component beyond the effective area to avoid the detection of its edges.

The details of Gabor filtering, as well as the results of single-scale and multiscale analysis obtained with retinal fundus images from the Digital Retinal Images for Vessel Extraction (Staal et al., 2004) (DRIVE) database are provided by Rangayyan et al. (Rangayyan et al., 2008). The accuracy of the results was determined in comparison with the ground-truth images of the vessels provided in the DRIVE database and quantified in terms of the area under the receiver operating characteristic (ROC) curve.

5.1.2 Modeling of the MTA

By using a large thickness value when detecting blood vessels using the Gabor filters, it is possible to emphasize the presence of the MTA, which is the thickest branch of the blood vessels in the retina (Oloumi et al., 2012c). The steps involved in single- and dual-parabolic modeling of the MTA, STA, and ITA are:

1. Obtaining the skeletons of the MTA, the ITA, and the STA:
   (a) Obtaining the Gabor magnitude response to represent the MTA (Rangayyan et al., 2008).
   (b) Separating the Gabor magnitude response image into its superior and inferior parts to represent the STA and the ITA, respectively.
   (c) Binarizing the Gabor magnitude response images of the MTA, the ITA, and the STA.
   (d) Skeletonizing the binary images.
   (e) Applying the morphological process of area open to filter the skeletons.
2. Detecting parabolas and semiparabolas using the GHT (Oloumi et al., 2012c):
   (a) Rotating each skeleton image by 180°, if the MTA opens to the left (i.e., the image is of the right eye).
   (b) Cropping each skeleton image horizontally.
   (c) Applying the GHT to the preprocessed skeleton images of the MTA, the STA, and the ITA.
   (d) Rotating the Hough spaces by 180°, if the MTA opens to the left, and obtaining the parameters of the best-fitting parabolas.

Please refer to (Oloumi et al., 2012c) for details of the modeling methods, as well as the results of evaluation of the obtained parabolic models as compared to hand-drawn traces of the MTA.

Figure 1 shows the results of detection of the MTA using Gabor filters, as well as the results of single- and dual-parabolic modeling of the MTA, STA, and ITA using the GHT.

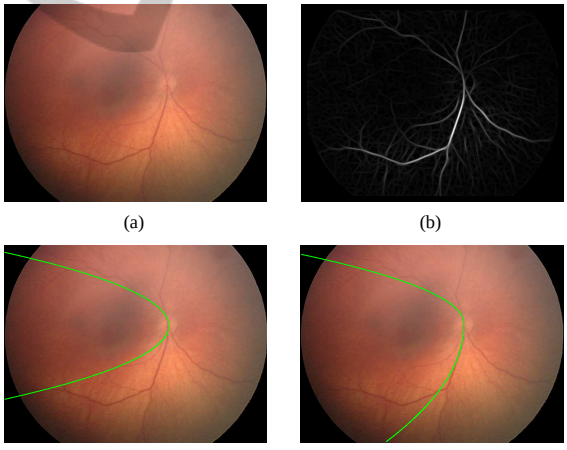

Figure 1: (a) Image 1701 of the TROPIC database. (b) Results of Gabor filtering with a bank of 90 filters spaced evenly over the range $[-\pi/2, \pi/2]$. (c) Single-parabolic model with $a_{\mathrm{MTA}} = -20$. (d) Dual-parabolic model with $a_{\mathrm{STA}} = -18$ and $a_{\mathrm{ITA}} = -108$.

5.1.3 A Graphical User Interface

By providing user guidance over the variables used in the detection and modeling procedures, it may be possible to reduce the modeling error and improve the accuracy of the related measures (Oloumi et al., 2012b). A GUI is being developed and tested in consultation

with a pediatric ophthalmologist and retinal specialist (Dr. A. L. Ells), and adheres to the main principles of GUI development, such as human factors, knowledge of the user's requirements and expectations, ease of use, intuitiveness, error handling capabilities, and proper documentation (Oloumi et al., 2012b; Oloumi et al., 2012a). The GUI contains a separate module for the three main steps of detection, binarization, and modeling of the MTA. The GUI also contains a module for measurement of the angle of insertion of the MTA, using the methods of Wilson et al. (Wilson et al., 2006) and Wong et al. (Wong et al., 2011).

5.1.4 Selection of Cases from the TROPIC Database

The TROPIC database contains images of 44 patients, with the possibility of multiple visits for each patient. The database contains images of both eyes of each patient. The TROPIC database does not contain images of Stages 4 and 5 ROP. Currently, 110 images (30 images for each of Stages 0, 1, and 2 and 20 images of Stage 3) have been selected from the database. At most, two images of the same patient were included for the same stage of ROP: one image from each eye. Images of the same eye from the same patient were included only if the ROP stages were different at the time of imaging. A total of 20 cases were also diagnosed with plus disease, which were categorized as Stages 2 and 3 of ROP. See (Oloumi et al., 2012d) for more information on the TROPIC database.

5.2 Future Work

5.2.1 Automated Detection of the Blood Vessels

The parameters of the previously developed methods for the detection of blood vessels have been optimized for use with the DRIVE database, which contains retinal fundus images of adults. The images of the TROPIC database are taken from preterm infants and have different characteristics in terms of spatial resolution, angle of field of view (FOV), thickness of the blood vessels, presence of choroidal vessels, and retinal pigmentation. It is necessary to optimize the parameters of the blood vessel detection methods for use with the TROPIC database.

The parameters used for thresholding of the grayscale images, needed for generation of the mask, will need to be optimized for the TROPIC database. A fixed thresholding value may be determined empirically; however, such a value may not work well for the images of the TROPIC database, because the images of preterm infants vary widely in terms of intensity and pigmentation. The average of pixel intensity values for a set of pixels at the center of the FOV and a set of border pixels (outside of the FOV) may be calculated for each image and a threshold level may be determined based on the two obtained averages.

Gabor filters are sensitive to oriented features, and since the boundary of the ONH (optic cup) represents an oval shape, which provides contrast (edges) between the darker retinal surface and the brighter area inside the ONH, it is also detected as a pattern with oriented components. This fact is the cause for the largest number of false-positive pixels in the results of single-scale and multiscale analysis, as well as the binarization step. Methods that consider the approximate location of the center of the ONH and the oval boundary of optic disk, and use the Gabor angle output to track the vessels that originate from the ONH, will be employed to reduce the number of false-positive pixels around the ONH.

5.2.2 Automated Detection of the ONH

The method of Rangayyan et al. (Rangayyan et al., 2010) will be used to analyze the orientation field image (Gabor angle output) using phase portrait analysis (Rao and Jain, 1992) to detect the point of convergence of vessels, which will serve to detect the center of the ONH. The results will be evaluated using the test set and the previously marked centers of the ONH by obtaining the Euclidean distance between the two centers of the ONH (manually and automatically marked).

5.2.3 Automated Modeling of the MTA

In order to detect and emphasize the presence of the MTA, a large value for the thickness parameter (τ) of the Gabor filters will be used (determined empirically). The resulting Gabor magnitude output will be thresholded at a specific value to obtain a binary image that contains mainly the MTA. A fixed value for the threshold level may be determined empirically for all images, or an automated thresholding method, such as Otsu's method (Otsu, 1979), may be used for this purpose. Small segments still remaining after the binarization step will be removed using the morphological operation of area open. The resulting binary image will be reduced to one-pixel-thick lines using the morphological process of skeletonization (Arcelli and di Baja, 1996). The skeleton image will then be used with the GHT for the detection of parabolas and semiparabolas (Oloumi et al., 2012c) to model the MTA, STA, and ITA.

5.2.4 Measurement of Vessel Thickness

The single-scale Gabor magnitude output image or a discriminant image obtained using multiscale analysis will be thresholded to obtain a binary image, which should contain most of the blood vessels. The skeleton image of the binarized vessels will then be obtained. Next, the branching and end-points of the skeleton will be determined using morphological operations. By using the branching points and the end-points, the skeleton will be broken down into segments. For each segment, a sliding window will be defined and centered on each pixel on the skeleton in an iterative manner. A straight line will then be fitted to the portion of the line segment in the sliding window and then the normal to the fitted line will be determined. The corresponding skeleton pixel at the center of the window will be identified in the binary image of the vessels. Moving in both directions from the center-line pixel along the normal, pixels that belong to the vessels (white pixels) will be removed from the binary image (not the skeleton) until the boundary of the vessel is reached. The count of the number of pixels on the normal within the vessel boundary will be used with the spatial resolution of the images to calculate a thickness measure for that specific pixel. The process will be repeated for every pixel on the skeleton to obtain an overall measure of thickness. Preprocessing steps such as pruning and cleaning will be needed in order to decrease the effect of false-positive pixels on the thickness measure.

It should be noted that the thresholding level used to binarize the grayscale image could have an effect on the measured thickness of the vessels; however, as long as the thresholding level is consistent over the images of all stages, the relative changes in the thickness measure should remain the same for all images. A valid thresholding level may be determined by analyzing the histogram of the Gabor magnitude output or the discriminant image values (grayscale intensity) of the pixels that belong to the skeleton. Such a histogram will determine the range of intensity values of the pixels that belong to the center of each vessel; a suitable threshold value may be determined based on this range of values. Another method for the determination of a suitable thresholding value will be based on the ROC curve obtained for the grayscale image (single or multiscale result) versus the ground-truth image. The point on the ROC curve which is the closest to the point $(0,1)$ will provide the optimal threshold level.

5.2.5 Measurement of Vessel Tortuosity

Most of the methods in the literature that are used for the measurement of vessel tortuosity, as explained in Section 4.2, divide the detected vasculature into several segments, and for each segment, define the tortuosity as a measure that relates the total length of the line segment to the chord of the segment (a straight line connecting the tip of the segment to its tail). Such methods require the detection or derivation of edge information with regard to the blood vessels. In the present work, the Gabor filters used for the detection of the blood vessels provide a phase (angle) image, which indicates the dominant orientation for each pixel in the image. The Gabor phase angle information will be analyzed using a sliding window to determine the relationship between each pixel and its neighboring pixels; information such as the rate of change of the angle will be used to derive a tortuosity measure.

Assuming that a tortuous vessel, as compared to a straight vessel, has a higher complexity from the perspective of fractal analysis, the box-counting method for measurement of the fractal dimension (FD) (Peitgen et al., 2004) is expected show an increase in the FD of a case with plus disease (tortuous vessels), as compared to a case without plus disease (straight vessels). Such a measure may not directly quantify the level of tortuosity; however, the distinction between the FD of normal cases as compared to abnormal ones could be sufficient to discriminate between cases with and without plus disease.

5.2.6 Quantification of the MTA

The dual-parabolic modeling approach can be biased if the ITA or the STA have nonlinear rates of divergence. A parabola has a linear divergence rate controlled by the parameter *a*. The approximate shape of the overall architecture of the MTA may appear to be parabolic or semielliptical; however, upon close inspection, it is clear that the STA and the ITA are often asymmetric. More accurate modeling of each arcade may be possible by applying higher-order models. A high-order curve-fitting method may provide more accurate results in terms of modeling and parametrization of the STA and ITA. A high-order curve-fitting method such as the least-squares method (Kay, 1993) will be used to fit a second-order or higher-order model to the MTA, STA, and ITA.

Another possible method for quantification of the openness of the MTA is by obtaining the principal axis (Rangayyan, 2005) of the skeleton of the MTA and then obtaining various moments with respect to the Gabor angle information of the skeleton pixels and value of the principal axis.

5.2.7 Pattern Classification

The results of the modeling of the MTA as well as the thickness and tortuosity measures will be combined using linear and nonlinear pattern classification methods, such as quadratic discriminant analysis, multilayer neural networks, radial basis functions, and support vector machines (Duda et al., 2001), to obtain a single set of discriminatory values for the purpose of discrimination between various stages of ROP, including screening for ROP (no ROP versus ROP), staging of ROP, and diagnosis of plus disease. A training set of images will be used to train the classifiers, which will then be tested using an independent test set of images.

5.2.8 Testing and Diagnostic Evaluation

ROC analysis provides a measure of the decision performance of a feature by introducing two indices (Metz, 1978): sensitivity and specificity. The diagnostic accuracy of all the methods and features described and obtained in the proposed thesis work will be determined based on ROC analysis and the related A_z values. This includes determining the accuracy of the blood vessel detection algorithm, the discriminatory capabilities of the derived measures of thickness, tortuosity, and the parameters of the models of the MTA, STA, and ITA, as well as the discriminatory values obtained from the pattern classification techniques, as explained in Section 5.2.7.

Considering the fact that the sample size of the database of the selected images is relatively small, the method of leave-one-out will be used to train and test the classifiers. A bootstrap method will be used to establish the reliability of the obtained A_z values based on changes in the configuration and training protocols of the classifiers, as well as to determine the presence of possible inconsistent data (Efron and Tibshirani, 1994; **?**). The confidence and prediction intervals obtained using the bootstrap method could be used to optimize the configuration of the classifiers.

In order to determine the significance of the differences between the values of the obtained features (i.e., thickness measure, tortuosity measure, and openness parameter), as well as the differences between the values obtained for various stages of ROP for each feature (i.e., ROP versus no ROP and Stages $0+1$ versus Stages $2+3$), the p-value will be obtained via the t-test (Goodman, 1999).

6 PRELIMINARY RESULTS

Using the implemented GUI (see Section 5.1.3), the parabolic and dual-parabolic models of the MTA, STA, and ITA, as well as the arcade angle measures according to the method of Wong et al. (Wong et al., 2011) were obtained for a small set of images selected from the TROPIC database. The results indicate an area under the ROC curve of $A_z = 0.75$ using the results of single- and dual-parabolic modeling in the discrimination of Stage 0 ROP from Stage 3 ROP; $A_z = 0.71$ was obtained in screening for ROP (Stage 0 versus Stages $1, 2,$ and 3). The arcade angle provided similar results ($A_z = 0.74$). The p-values for the screening purpose indicate a statistically significant difference between the values of the parabolic models, as well as the arcade angles, for Stage 0 versus Stages $1, 2,$ and 3, and Stage 0 versus Stages 2 and 3. See (Oloumi et al., 2012d) for details of the obtained results in terms of A_z and p-values. This analysis will be completed by using all available cases in the TROPIC database as part of the proposed thesis work.

The changes that affect the architecture of the MTA in the presence of ROP also appear as side effects of proliferative diabetic retinopathy (PDR). Using 22 images from the STructured Analysis of the REtina (STARE) database, where 11 of the images were diagnosed with PDR, the results obtained using the openness parameters of single- and dual-parabolic models as well as the arcade angle measurements indicate areas under the ROC curves of $A_z = 0.94, 0.87,$ and 0.84, respectively. See (Oloumi et al., 2013) for details of the obtained results in terms of A_z and p-values. Although the results are encouraging, a larger number of cases of PDR are needed for further analysis; however, the number of publicly available databases of retinal images that provide diagnostic information is limited.

7 EXPECTED OUTCOME

As described in Section 4.2, it has been shown that the changes in vessel thickness and tortuosity in the presence of plus disease can be detected and used by CAD systems for the diagnosis of plus disease and hence, active ROP. It is expected that the proposed novel methods for the quantification of features of the MTA and retinal vasculature (see Sections 5.2.4 and 5.2.5) will provide better results. By combining the results of quantification of the openness of the MTA with the thickness and tortuosity measures using pattern classification methods, we expect to obtain better

results in the diagnosis of ROP and plus disease.

REFERENCES

Arcelli, C. and di Baja, G. S. (1996). Skeletons of planar patterns. In TY, K. and A, R., editors, *Topological Algorithms for Digital Image Processing*, volume 19 of *Machine Intelligence and Pattern Recognition*, pages 99–143. North-Holland, Amsterdam, The Netherlands.

Chiang, M. F., Jiang, L., Gelman, R., Du, Y. E., and Flynn, J. T. (2007). Interexpert agreement of plus disease diagnosis in retinopathy of prematurity. *Archives of Ophthalmology*, 125(7):875–880.

Cryotherapy for Retinopathy of Prematurity Cooperative Group (2001). Multicenter trial of cryotherapy for retinopathy of prematurity: Ophthalmological outcomes at 10 years. *Archives of Ophthalmology*, 119:1110–1118.

Duda, R. O., Hart, P. E., and Stork, D. G. (2001). *Pattern Classification*. Wiley, New York, NY, 2nd edition.

Efron, B. and Tibshirani, R. J. (1994). *An Introduction to the Bootstrap - Monographs on Statistics & Applied Probability*. Chapman and Hall/CRC, 1 edition.

Ells, A. L. and MacKeen, L. D. (2008). Dynamic documentation of the evolution of retinopathy of prematurity in video format. *Journal of American Association for Pediatric Ophthalmology and Strabismus*, 12(4):349–351.

Fiorin, D. and Ruggeri, A. (2011). Computerized analysis of narrow-field ROP images for the assessment of vessel caliber and tortuosity. In *Engineering in Medicine and Biology Society, 33rd Annual International Conference of the IEEE*, pages 2622–2625, Boston, MA.

Fleming, A. D., Goatman, K. A., Philip, S., Olson, J. A., and Sharp, P. (2007). Automatic detection of retinal anatomy to assist diabetic retinopathy screening. *Physics in Medicine and Biology*, 52:331–345.

Foracchia, M., Grisan, E., and Ruggeri, A. (2004). Detection of optic disc in retinal images by means of a geometrical model of vessel structure. *IEEE Transactions on Medical Imaging*, 23(10):1189–1195.

Gelman, R., Martinez-Perez, M. E., Vanderveen, D. K., Moskowitz, A., and Fulton, A. B. (2005). Diagnosis of plus disease in retinopathy of prematurity using retinal image multiscale analysis. *Investigative Ophthalmology & Visual Science*, 46(12):4734–4738.

Goodman, S. N. (1999). Toward evidence-based medical statistics. 1: The p value fallacy. *Annals of Internal Medicine*, 130(12):995–1004.

Heneghan, C., Flynn, J. T., O'Keefe, M., and Cahill, M. (2002). Characterization of changes in blood vessels width and tortuosity in retinopathy of prematurity using image analysis. *Medical Image Analysis*, 6(1):407–429.

Hildebrand, P. L., Ells, A. L., and Ingram, A. D. (2009). The impact of telemedicine integration on resource use in the evaluation ROP ... analysis of the telemedicine for ROP in Calgary (TROPIC) database. *Investigative Ophthalmology and Visual Sciences*, 50:E–Abstract 3151.

International Committee for the Classification of Retinopathy of Prematurity (2005). The international classification of retinopathy of prematurity revisited. *Archives of Ophthalmology*, 123:991–999.

Kay, S. M. (1993). Least squares. In *Fundamentals of Statistical Signal Processing, Volume I: Estimation Theory*, pages 219–286. Prentice Hall PTR.

Li, H. and Chutatape, O. (2004). Automated feature extraction in color retinal images by a model based approach. *IEEE Transactions on Biomedical Engineering*, 51(2):246–254.

Liu, K. Y., Smith, M. R., Fear, E. C., and Rangayyan, R. M. (2012). Evaluation and amelioration of computer-aided diagnosis with artificial neural networks utilizing small-sized sample sets. *Biomedical Signal Processing and Control*, Online:8. In press.

Metz, C. E. (1978). Basic principles of ROC analysis. *Seminars in Nuclear Medicine*, VIII(4):283–298.

Oloumi, F., Rangayyan, R. M., and Ells, A. L. (2012a). A graphical user interface for measurement of temporal arcade angles in fundus images of the retina. In *Canadian Conference on Electrical and Computer Engineering (CCECE), Proc. IEEE Canada 25th Annual*, pages 4 on CD–ROM, Montreal, QC, Canada.

Oloumi, F., Rangayyan, R. M., and Ells, A. L. (2012b). A graphical user interface for measurement of the openness of the retinal temporal arcade. In *Medical Measurements and Applications (MeMeA), Proc. IEEE International Symposium on*, pages 238–241, Budapest, Hungary.

Oloumi, F., Rangayyan, R. M., and Ells, A. L. (2012c). Parabolic modeling of the major temporal arcade in retinal fundus images. *IEEE Transactions on Instrumentation and Measurement (TIM)*, 61(7):1825–1838.

Oloumi, F., Rangayyan, R. M., and Ells, A. L. (2012d). Quantitative analysis of the openness of the major temporal arcade in retinal fundus images of retinopathy of prematurity. In *The First International Conference on Emerging Research in Electronics, Computer Science and Technology*, Leture Notes in Electrical Engineering, pages 829–842, Mandya, Karnataka, India. Springer, LNEE.

Oloumi, F., Rangayyan, R. M., and Ells, A. L. (2013). Quantitative analysis of the major temporal arcade in retinal fundus images of preterm infants for detection of plus disease. In *The 15th International Association of Science and Technology for Development (IASTED) Conference on Signal and Image Processing*, Banff, Alberta, Canada.

Otsu, N. (1979). A threshold selection method from gray-level histograms. *IEEE Transactions on Systems, Man and Cybernetics*, SMC-9:62–66.

Peitgen, H. O., Jurgens, H., and Saupe, D. (2004). *Chaos and Fractals: New Frontiers of Science*. Springer-Verlag, New York, NY.

Poletti, E., Grisan, E., and Ruggeri, A. (2012). Image-level tortuosity estimation in wide-field retinal images from infants with retinopathy of prematurity. In *Engineering in Medicine and Biology Society, 34th Annual*

International Conference of the IEEE, pages 4958–4961, San Diego, CA.

Rangayyan, R. M. (2005). *Biomedical Image Analysis*. CRC, Boca Raton, FL.

Rangayyan, R. M., Ayres, F. J., Oloumi, F., Oloumi, F., and Eshghzadeh-Zanjani, P. (April-June 2008). Detection of blood vessels in the retina with multiscale Gabor filters. *Journal of Electronic Imaging*, 17:023018:1–7.

Rangayyan, R. M., Zhu, X., Ayres, F. J., and Ells, A. L. (2010). Detection of the optic nerve head in fundus images of the retina with Gabor filters and phase portrait analysis. *Journal of Digital Imaging*, 23(4):438–453.

Rao, A. R. and Jain, R. C. (1992). Computerized flow field analysis: Oriented texture fields. *IEEE Transactions on Pattern Analysis and Machine Intelligence*, 14(7):693–709.

Staal, J., Abràmoff, M. D., Niemeijer, M., Viergever, M. A., and van Ginneken, B. (2004). Ridge-based vessel segmentation in color images of the retina. *IEEE Transactions on Medical Imaging*, 23(4):501–509.

Tobin, K. W., Chaum, E., Govindasamy, V., and Karnowski, T. P. (2007). Detection of anatomic structures in human retinal imagery. *IEEE Transactions on Medical Imaging*, 26(12):1729–1739.

Wallace, D. K., Quinn, G. E., Freedman, S. F., and Chiang, M. F. (2008). Agreement among pediatric ophthalmologists in diagnosing plus and pre-plus disease in retinopathy of prematurity. *Journal of American Association for Pediatric Ophthalmology and Strabismus*, 12(4):352–356.

Watzke, R. C., Robertson, J. E., Palmer, E. A., Wallace, P. R., Evans, M. S., and Soldevilla, J. E. D. (1990). Photographic grading in the retinopathy of prematurity cryotherapy trial. *Archives of Ophthalmology*, 108(7):950–955.

Welfer, D., Scharcanski, J., Kitamura, C. M., Pizzol, M. M. D., Ludwig, L. W. B., and Marinho, D. R. (2010). Segmentation of the optic disk in color eye fundus images using an adaptive morphological approach. *Computers in Biology and Medicine*, 40(2):124–137.

Wilson, C. M., Cocker, K. D., Moseley, M. J., Paterson, C., Clay, S. T., Schulenburg, W. E., Mills, M. D., Ells, A. L., Parker, K. H., Quinn, G. E., Fielder, A. R., and Ng, J. (2008). Computerized analysis of retinal vessel width and tortuosity in premature infants. *Investigative Ophthalmology and Visual Science*, 49(1):3577–3585.

Wilson, C. M., Theodorou, M., Cocker, K. D., and Fielder, A. R. (2006). The temporal retinal vessel angle and infants born preterm. *British Journal of Ophthalmology*, 90:702–704.

Wong, K., andA. L. Ells, J. N., Fielder, A. R., and Wilson, C. M. (2011). The temporal and nasal retinal arteriolar and venular angles in preterm infants. *British Journal of Ophthalmology*, 95(12):1723–1727.

Ying, H. and Liu, J. C. (2010). Automated localization of macula-fovea area on retina images using blood vessel network topology. In *Acoustics Speech and Signal Processing, IEEE International Conference on*, pages 650–653.